IEEE Photonics Journal
An IEEE Photonics Society Publication

Open Access

Magnetic Field Sensor Based on U-Bent Single-Mode Fiber and Magnetic Fluid

Volume 6, Number 6, December 2014

Tiegen Liu
Yaofei Chen
Qun Han
Xiaoying Lü

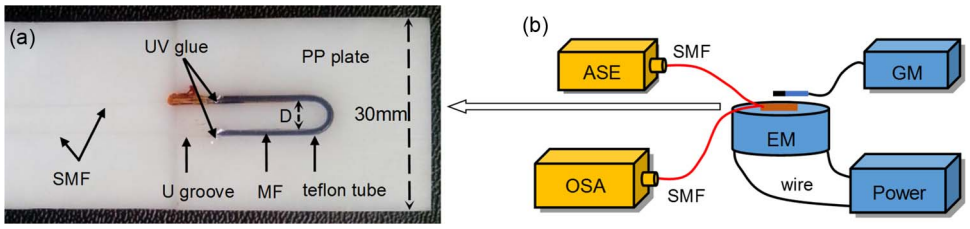

DOI: 10.1109/JPHOT.2014.2368781
1943-0655 © 2014 IEEE

Magnetic Field Sensor Based on U-Bent Single-Mode Fiber and Magnetic Fluid

Tiegen Liu,[1,2] Yaofei Chen,[1] Qun Han,[1] and Xiaoying Lü[1]

[1]College of Precision Instrument and Opto-Electronics Engineering, Tianjin University, Tianjin 300072, China
[2]Key Laboratory of Opto-Electronics Information Technology of Ministry of Education, Tianjin University, Tianjin 300072, China

DOI: 10.1109/JPHOT.2014.2368781
1943-0655 © 2014 IEEE. Translations and content mining are permitted for academic research only. Personal use is also permitted, but republication/redistribution requires IEEE permission. See http://www.ieee.org/publications_standards/publications/rights/index.html for more information.

Manuscript received October 13, 2014; revised October 31, 2014; accepted November 2, 2014. Date of publication November 10, 2014; date of current version November 25, 2014. This work was supported in part by the Natural Science Foundation of Tianjin under Grant 13JCYBJC16100, by the National Natural Science Foundation of China under Grant 61107035 and Grant 61378043, by the National Key Scientific Instrument and Equipment Development Project of China under Grant 2013YQ03091502, and by the National Basic Research Program of China (973 Program) under Grant 2014CB340104. Corresponding author: Q. Han (e-mail: hanqun@tju.edu.cn).

Abstract: In this paper, an all-fiber magnetic field sensor based on a U-bent single-mode fiber and magnetic fluid (MF) is proposed and investigated. Because of the tunable refractive index and absorption coefficient of MF, the transmission spectrum will change with the magnetic field strength (H), which can be used to demodulate H through the wavelength shift or the intensity change. The influence of the diameter of the U shape to the performance of the sensor is investigated and discussed. In the experiments, the highest sensitivities achieved with wavelength and intensity demodulation are 0.374 nm/Oe and −0.4821 dB/Oe, respectively. The reproducibility of the sensor is studied as well.

Index Terms: Optical fiber sensors, bent single mode fiber, magnetic field sensing, magnetic fluids.

1. Introduction

The measurement of magnetic field is very important in the many fields, such as navigation, aerospace, environmental monitoring, and smart grids, etc. Compared to electronic techniques employed in magnetic field detection, fiber-based magnetic field sensors have advantages of immunity to electromagnetic interference, small size, and low loss for long distance operation etc. [1]. To date various kinds of fiber-based magnetic field sensor have been reported. It can be realized by a magnetostrictive composite-FBG structure [2], [3], coating TbDyFe thin films on an etched FBG [4], or utilizing the Faraday effect in a highly terbium-doped fiber [5], etc. These sensors have such advantages as high precise, fast response (e.g., over 60 kHz response frequency in [2]), and large measurement range (e.g., 0.02 to 3.2 T in [5]).

On the other hand, magnetic fluid (MF), a stable colloidal suspension of ferromagnetic nanoparticles in certain suitable liquid carriers, has attracted considerable interests recently in magnetic field sensing when combining with a suitable fiber structure. Based on the various outstanding magneto-optic properties of MF such as tunable refractive index (RI), birefringence, and tunable absorption coefficient [6], [7], several kinds of all-fiber magnetic field sensors have

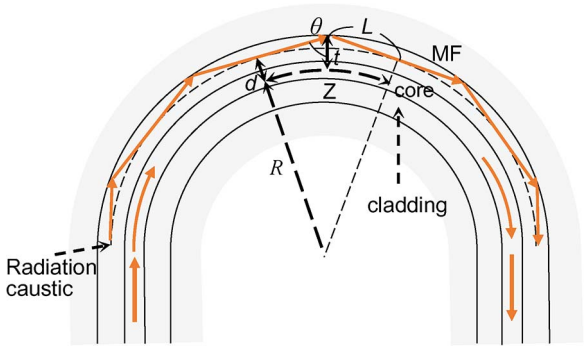

Fig. 1. Schematic diagram of the sensor based on U-bent SMF and MF.

been proposed [8]–[13]. Compared with other materials for fiber magnetic sensors, such as the magnetostrictive materials [2]–[4], and the terbium-doped fiber [5], MF is easier to integrate with a fiber. Nevertheless, in the previously reported MF-based fiber magnetic sensors, either a special fiber (such as LPFG with D-shaped fiber [8], photonic crystal fiber [12], and no-core fiber [6], [13]) or a special structure (such as s-tapered microfiber [9], fiber with up-tapered joints [10], and microfiber knot [11]) is needed. Compared to these cases, the interferometer induced from a bent single-mode fiber (SMF), based on the interference between the whispering gallery mode (WGM) and the core mode [14], can be more easily achieved by mechanically bending an SMF to a radius of curvature of several millimeters. Since the WGM is susceptible to external parameters, the bent-SMF based interferometers can be used to detect temperature [15], and RI [16] etc. It will be a promising method to realize the magnetic field sensing if we combine the MF with a bent-SMF structure.

In this paper, we propose and investigate an all-fiber magnetic field sensor based on U-bent SMF and MF. The sensor can be simply fabricated by bending a piece of coating-stripped-SMF to a radius of curvature of several millimeters. The MF is used to act as the coating of the U-bent SMF. Because of the tunable RI and absorption coefficient of MF, the transmission spectrum of the sensor will change with the magnetic field, which in turn can be used to demodulate the magnetic field by monitoring the dip wavelength or light intensity. The influence of the diameter of the U-shape to the sensor's performance is investigated. The repeatability of the results is also verified experimentally. Compared with our previous work, in which a U-bent single-mode-no-core-single-mode structure with an MF cladding was fabricated to sense the magnetic field (sensitivities: 0.319 nm/Oe and 0.56 dB/Oe) [13], the sensor proposed here not only has the advantages of lower cost and easier fabrication (only a piece of SMF is needed) but has the comparative sensitivities to magnetic field as well (0.374 nm/Oe and –0.4821 dB/Oe).

2. Working Principles

Fig. 1 shows the schematic diagram of the sensor. A piece of coating-stripped SMF is bent to a U-shape and the MF is used to serve as the coating of the SMF. When the light bounded in the core of the straight SMF propagates to the bent section, the light beyond the radiation caustic will be free from the constraint of the core and penetrate into the cladding. If the RI of MF is smaller than that of the cladding and the radius of the U-shape is not too small, total reflection will occur at the cladding-MF boundary and form the so-called WGM [17], as shown in Fig. 1. After passing through the U-bent section along the wall of the cladding, the WGM will couple back to the core mode. Thus mode interference occurs in the straight lead-out SMF.

Assuming I_{core} and I_{wis} represent the light intensity of the core mode and the WGM in the U-bent SMF, respectively, the output light intensity at wavelength λ can be described as

$$I(\lambda) = I_{core} + I_{wis} + 2\sqrt{I_{core} I_{wis}} \cos\varphi \quad (1)$$

where φ is the phase difference between the core mode and the WGM. Depending on the ray theory, it can be expressed as [14]

$$\varphi = N\left(2\pi n_{\text{clad}}\frac{2L}{\lambda} + \varphi_r - Z\beta\right) \tag{2}$$

where N is the number of reflections of the WGM on the cladding-MF boundary in the U-bent section; n_{clad} is the RI of SMF's cladding; β is the propagation constant of the fundamental mode in the straight SMF; φ_r is the phase change of the total reflection on the cladding-MF boundary. Z is the arc length in the core between two points of contact as shown in Fig. 1; L is the half path length between two reflection points and can be given by

$$L = \sqrt{(R+t)^2 - (R+d)^2} \tag{3}$$

where R is the bending radius of the fiber in the U-shape section, t is the distance from the cladding-MF interface to the core axis, and d is the distance between the radiation caustic and the core axis. d can be calculated by [17]

$$d = R\left(\frac{\beta\lambda}{2\pi n_{\text{clad}}} - 1\right). \tag{4}$$

If a broad-band light is injected into one end of the sensor, an interference fringe in the wavelength domain can be got from the other end. For the dips/peaks in the fringe, φ in (2) should be equal to $m\pi$, where m is an integer. For an SMF, it is reasonable to assume that d is independent on λ at a small wavelength range. Then deriving from (2), the response of the dip/peak wavelength to the RI of MF (n_{MF}) can be expressed as

$$\frac{\mathrm{d}\lambda_{\text{dip/peak}}}{\mathrm{d}n_{\text{MF}}} = \frac{4\pi n_{\text{clad}} L}{[m\pi/N + Z\beta - \varphi_r]^2}\cdot\frac{\mathrm{d}\varphi_r}{\mathrm{d}n_{\text{MF}}}. \tag{5}$$

From (1), the light intensity at the peak wavelength can be described as

$$I_{\text{peak}} = (\sqrt{I_{\text{core}}} + \sqrt{I_{\text{wis}}})^2. \tag{6}$$

Because the RI of MF changes with the magnitude of an applied magnetic field [9], it can be known from (5) that the dip/peak wavelength will shift with the change of the applied magnetic field as well. Thus the magnetic field can be demodulated from the dip/peak wavelength shift. On the other hand, since the absorption coefficient of MF increases with the increase of applied magnetic field, I_{wis} will decrease consequently because of the evanescent field absorption [6]. From (6), we can see that the I_{peak} will also decrease with the increase of applied magnetic field. This provides us another demodulation method by monitoring the intensity at a specific wavelength, which should be around the peak wavelength.

3. Experiments and Discussions

Fig. 2(a) is the photo of one sensor. First, a U-shape groove with 1 mm depth and 1 mm width is etched on a $75 \times 30 \times 7$ mm polypropylene (PP) plate. Then a piece of coating-stripped SMF (SMF-28, Corning Inc.) with 30 mm length is fed into the center of a Teflon tube with a length of 40 mm and an inner/outer diameter of 0.6/1 mm. The Teflon tube, together with the SMF, is bent and fixed into the U-shape groove, and the MF (EMG-605, Ferrotec Inc.) with a RI about 1.40 [6] is injected into the tube by an injector. Lastly, the two ends of the tube are sealed with UV glue to avoid the leakage of MF.

Three sensors with different diameters of the U-shape [marked as D in the Fig. 2(a)] are fabricated and tested. The Ds of the three sensors are 8, 6, and 4 mm, respectively. Fig. 2(b) shows the schematic diagram of the experimental setup for sensor characterization. A broadband light source (ASE, LightComm Ltd.) and an optical spectrum analyzer (Advantest Q8384) are used to

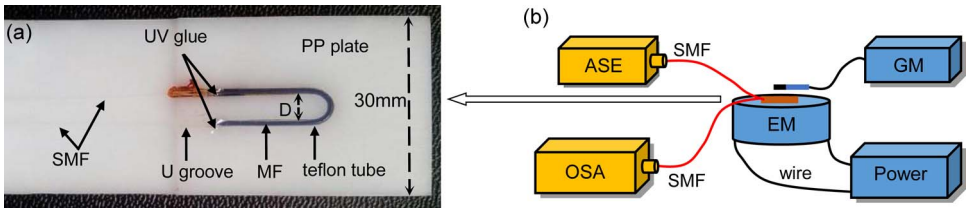

Fig. 2. (a) The picture of one sensor. (b) Schematic diagram of experimental setup. PP, polypropylene; ASE, amplified spontaneous emission; OSA, optical spectrum analyzer; EM, electromagnet; GM, gaussmeter.

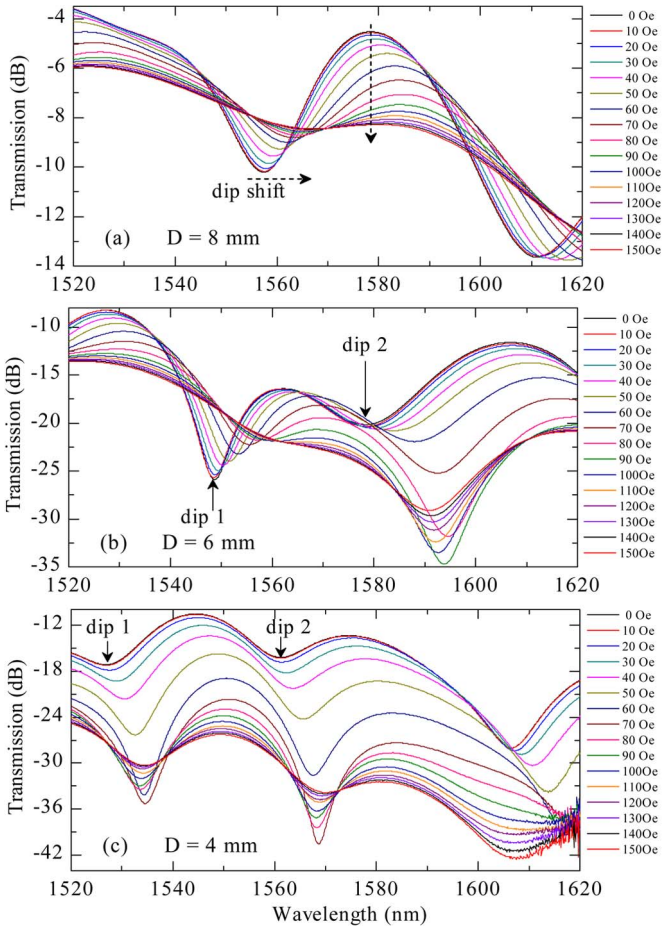

Fig. 3. The transmission spectra responses of sensors with the diameter of U-shape of (a) 8, (b) 6, and (c) 4 mm to the magnetic field, respectively.

record the transmission spectrum. The magnetic field is provided by an electromagnet and the magnetic field strength is controlled by adjusting the passing current. The direction of applied magnetic field is perpendicular to the surface of the PP plate. During the experiments, the ambient temperature is kept at 24 °C.

Fig. 3(a)–(c) show the responses of the transmission spectra of the three sensors to the magnetic field strength (H) when H changes from 0 to 150 Oe. It can be found that there is one, two, and two dips in the transmission spectrum for the sensor with a D of 8, 6, and 4 mm, respectively. As we predicted in the principle section, on one hand all the dips shift with the change of the magnetic field because of the tunable RI of MF. On the other hand, the intensities

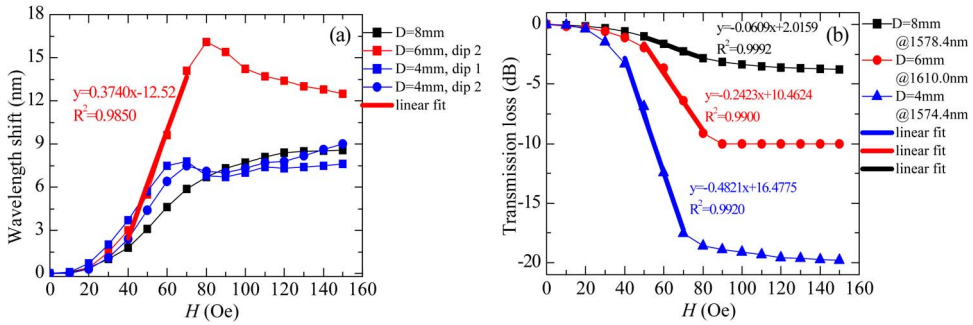

Fig. 4. (a) Wavelength shifts of dips with the change of H. (b) Transmission loss versus H at the specific wavelengths.

of the peaks decrease with the increase of the magnetic field because of the tunable absorption coefficient of MF.

Fig. 4(a) shows the wavelength shifts of the dips with the change of H. It should be pointed out that dip 1 in Fig. 3(b) will disappear when H is over 100 Oe; therefore, the wavelength shift depending on H is not plotted in Fig. 4(a) for dip 1 when D is 6 mm. First, it can be found that for the sensor with $D = 8$ mm, the dip keeps shifting to longer wavelength with the increase of H; However, for the other two sensors with $D = 6$ and 4 mm, the dips do not always move to longer wavelength as H being increased but exhibit a blue shift after a certain H. This phenomenon can be ascribed to the influence of polarization. When D is relatively large, 8 mm for example, the angle θ shown in Fig. 1 will be large enough to make φ_r in (5) ignore the influence of wave polarization and φ_r can be simply given by [18]

$$\varphi_r = -2\tan^{-1}\left\{\frac{\left[n_{\text{clad}}^2 - n_{\text{MF}}^2\right]^{\frac{1}{2}}}{n_{\text{clad}}\cot\theta}\right\}. \tag{7}$$

Substituting (7) into (5), it can be found that $\mathrm{d}\lambda_{\text{dip/peak}}/\mathrm{d}n_{\text{MF}} > 0$, which means that the dip/peak will shift to longer wavelength with H monotonically. However, a smaller D, namely a smaller R, will lead to a smaller θ, which can be seen from the expression of

$$\tan\theta = \left\{\left[\left(1 + \frac{t}{R}\right)\frac{2\pi n_{\text{clad}}}{\beta\lambda}\right]^2 - 1\right\}^{-\frac{1}{2}}. \tag{8}$$

Equation (8) can be derived from (3) and (4) depending on the geometrical relationship shown in Fig. 1. When D is relatively smaller, e.g., 6 and 4 mm, the wave polarization can't be ignored due to the smaller θ. Thus φ_r can't be simply expressed as (7), and it must be analyzed depending on TE and TM mode separately as shown in [19]. However, the TE and TM mode have different responses to H because of the birefringence of MF [20], which will contribute to the blue shift of the dips as we see in Fig. 3(b) and (c). Therefore, in practical applications, it is preferable to choose a relatively larger D, which can eliminate the effect of polarization. Secondly, the responses of dip 1 and dip 2 to H when $D = 4$ mm are different as shown in Fig. 4(a). This can be explained by the fact that more than one WGM will be excited in the U-sent section. From Fig. 4(a), we can see that the highest sensitivity, 0.374 nm/Oe, has been achieved in the linear range from 40 to 70 Oe when $D = 6$ mm.

Fig. 4(b) shows the transmission loss of the three sensors versus H at specific wavelengths. The selection of the specific wavelengths is based on the principle that at these wavelengths, the transmission not only change monotonically with H but has the largest change as well. According to this criteria, 1578.4, 1610.0, and 1574.4 nm are selected for the three sensors with $D = 8$, 6, and 4 mm, respectively. These wavelengths are all around the peak wavelength as shown in Fig. 3. From Fig. 4(b), we can see that the transmission losses decrease monotonically with the

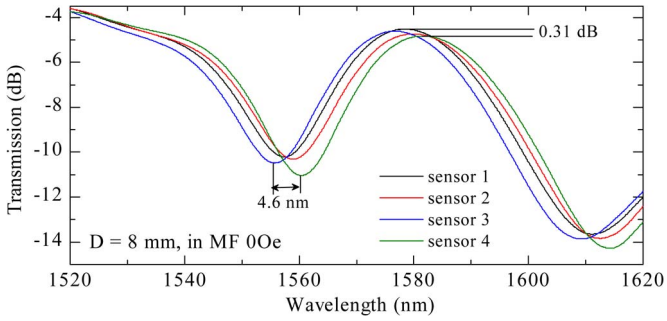

Fig. 5. Transmission spectra of four sensors when the D is 8 mm and H is 0 Oe.

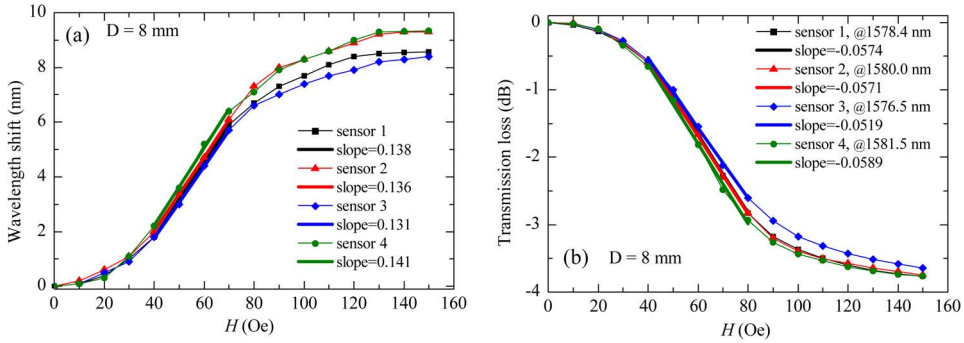

Fig. 6. (a) Wavelength shifts of dips of different sensors depending on H. (b) Transmission losses versus H at the specific wavelengths.

increase of H for all of the three sensors. Besides, it can be found that the sensitivity to H increases with the decrease of D, and in the linear range from 40 to 70 Oe, the highest sensitivity is −0.4821 dB/Oe for the sensor with $D = 4$ mm. This phenomenon can be explained from (4) that a smaller D, namely a smaller R, will result in a smaller d, which means that more light will enter the cladding and form the WGM. Consequently, more light will interact with the MF through the evanescent field of the WGM, thus the sensitivity will be enhanced.

To assess the repeatability of the results, using the same materials, we have fabricated and tested another three sensors with the same D of 8 mm. Fig. 5 shows the transmission spectra of the three sensors together with the one with $D = 8$ mm used in the former experiment when all of them are immersed in MF with $H = 0$ Oe. We can see that they overlap with each other fair well except a little deviation. The largest differences of the dip wavelengths and peak intensities of the four sensors are 4.6 nm and 0.31 dB, respectively, as shown in the Fig. 5. Decreasing the width of U-shape groove and the diameter of Teflon tube can help to reduce such differences and increase the reproducibility in sensor fabrication.

Fig. 6(a) and (b) show the dip wavelength shifts and the transmission losses at the specific wavelengths versus H for the four sensors with the same D of 8 mm, respectively. We can see that the lines are consistent with each other fair well, although a small deviation exists. The linear fittings are carried out in the linear range. The results show that the largest differences of the slopes are 0.01 and 0.007, as shown in the Fig. 6(a) and (b), respectively.

It is worth noting that either the U-bent SMF [15] or the RI of MF [13] is also sensitive to temperature. To ensure a good accuracy, the influence of temperature must be properly compensated. This can be done by introducing another temperature sensor, e.g., a FBG temperature sensor [21], to measure the temperature. The size of the sensor mainly depends on the size of the package, i.e., the PP plate $(75 \times 30 \times 7$ mm$)$ in this paper, and it can be designed according to the need of a specific application, as long as D can be ensured.

4. Conclusion

In summary, an all-fiber magnetic field sensor based on U-bent SMF and MF has been proposed and investigated. The sensor possesses the advantages of low cost, easy fabrication, small size, and high sensitivity. The underlying principle is described and the characteristics of the sensor are predicted in the principle section. In the experimental section, several sensors with different diameters (D) of U-shape groove are fabricated and tested. We found that the transmission spectra of the sensors will change with the increase of the magnetic field strength (H), which can be used to demodulate H through the wavelength shift or the intensity change. For wavelength demodulation, the shifts of the dip wavelengths for the sensors with different Ds are different, and the highest sensitivity of 0.374 nm/Oe has been achieved. For intensity demodulation, the sensitivity will increase with the decrease of D, and the highest sensitivity of −0.4821 dB/Oe is achieved. In addition, three more sensors with the same Ds are fabricated and tested. The results indicate that the proposed sensor has a good reproducibility.

References

[1] W. Jixuan *et al.*, "Dual-direction magnetic field sensor based on core-offset microfiber and ferrofluid," *IEEE Photon. Technol. Lett.*, vol. 26, no. 15, pp. 1581–1584, Aug. 2014.

[2] H. Liu, S. Wing, and H. Y. Tam, "Magnetostrictive composite-fiber Bragg grating (MC-FBG) magnetic field sensor," *Sens. Actuators A, Phys.*, vol. 173, no. 1, pp. 122–126, Nov. 2011.

[3] Q. Zhao *et al.*, "Femtosecond laser ablation of microstructures in fiber and application to magnetic field sensing," *Opt. Lett.*, vol. 39, no. 7, pp. 1905–1908, Feb. 2014.

[4] M. Yang, J. Dai, C. Zhou, and D. Jiang, "Optical fiber magnetic field sensors with TbDyFe magnetostrictive thin films as sensing materials," *Opt. Exp.*, vol. 17, no. 23, pp. 20 777–20 782, Nov. 2009.

[5] L. Sun, S. Jiang, and J. R. Marciante, "All-fiber optical magnetic-field sensor based on Faraday rotation in highly terbium-doped fiber," *Opt. Exp.*, vol. 18, no. 6, pp. 5407–5412, Mar. 2010.

[6] Y. Chen, Q. Han, T. Liu, X. Lan, and H. Xiao, "Optical fiber magnetic field sensor based on single-mode-multimode-single-mode structure and magnetic fluid," *Opt. Lett.*, vol. 38, no. 20, pp. 3999–4001, Oct. 2013.

[7] L. Gao, T. Zhu, J. Zeng, and K. S. Chiang, "Temporal response measurement of magnetic fluids based on D-shaped fiber intermodal interferometer," *Appl. Phys. Exp.*, vol. 6, no. 5, May 2013, Art. ID. 052502.

[8] L. Gao, T. Zhu, M. Deng, K. S. Chiang, and X. Sun, "Long-period fiber grating D-shaped fiber using magnetic fluid for magnetic-field detection," *IEEE Photon. J.*, vol. 4, no. 6, pp. 2094–2105, Dec. 2012.

[9] Y. Miao *et al.*, "Magnetic field tunability of optical microfiber taper integrated with ferrofluid," *Opt. Exp.*, vol. 21, no. 24, pp. 29 914–29 920, Dec. 2013.

[10] S. Pu and S. Dong, "Magnetic field sensing based on magnetic-fluid-clad fiber-optic structure with up-tapered joints," *IEEE Photon. J.*, vol. 6, no. 4, pp. 1–6, Aug. 2014.

[11] X. Li and H. Ding, "All-fiber magnetic-field sensor based on microfiber knot resonator and magnetic fluid," *Opt. Lett.*, vol. 37, no. 24, pp. 5187–5189, Dec. 2012.

[12] R. Gao, Y. Jiang, and S. Abdelaziz, "All-fiber magnetic field sensors based on magnetic fluid-filled photonic crystal fibers," *Opt. Lett.*, vol. 38, no. 9, pp. 1539–1541, May 2013.

[13] R. Zhang, T. Liu, Q. Han, Y. Chen, and L. Li, "U-bent single-mode-multimode-single-mode fiber optic magnetic field sensor based on magnetic fluid," *Appl. Phys. Exp.*, vol. 7, no. 7, Jul. 2014, Art. ID. 072501.

[14] S. H. Nam, "Whispering gallery mode and cladding mode resonance in optical fibers," Ph.D. dissertation, Penn. State Univ., Central County, PA, USA, 2005.

[15] S. H. Nam and S. Yin, "High-temperature sensing using whispering gallery mode resonance in bent optical fibers," *IEEE Photon. Technol. Lett.*, vol. 17, no. 11, pp. 2391–2393, Nov. 2005.

[16] G. Liu *et al.*, "Bent optical fiber taper for refractive index detection with a high sensitivity," *Sens. Actuators A, Phys.*, vol. 201, pp. 352–356, Aug. 2013.

[17] A. Harris and P. F. Castle, "Bend loss measurements on high numerical aperture single-mode fibers as a function of wavelength and bend radius," *J. Lightw. Technol.*, vol. 4, no. 1, pp. 34–40, Jan. 1986.

[18] Y. Murakami and H. Tsuchiya, "Bending losses of coated single-mode optical fibers," *IEEE J. Quantum Electron.*, vol. QE-14, no. 7, pp. 495–501, Jul. 1978.

[19] Q. Wang, G. Rajan, P. Wang, and G. Farrell, "Polarization dependence of bend loss for a standard singlemode fiber," *Opt. Exp.*, vol. 15, no. 8, pp. 4909–4920, Apr. 2007.

[20] P. Zu *et al.*, "Magneto-optical fiber sensor based on magnetic fluid," *Opt. Lett.*, vol. 37, no. 3, pp. 398–400, Feb. 2012.

[21] Y. Zhao, R. Q. Lv, D. Wang, and Q. Wang, "Fiber optic Fabry–Perot magnetic field sensor with temperature compensation using a fiber Bragg grating," *IEEE Trans. Instrum. Meas.*, vol. 63, no. 9, pp. 2210–2214, May 2014.